ResearchGate

See discussions, stats, and author profiles for this publication at: https://www.researchgate.net/publication/301599745

Trap-assisted large gain in Cu2O/C60 hybrid ultraviolet/visible photodetectors

Article *in* Applied Physics Letters · April 2016

DOI: 10.1063/1.4947581

CITATIONS
3

READS
39

9 authors, including:

Zisheng Su
Changchun Institute of Optics, Fine Mechanic…
100 PUBLICATIONS **1,302** CITATIONS
SEE PROFILE

Jingwei Xu
HERE
58 PUBLICATIONS **879** CITATIONS
SEE PROFILE

All content following this page was uploaded by Zisheng Su on 17 June 2016.

The user has requested enhancement of the downloaded file. All in-text references underlined in blue are added to the original document and are linked to publications on ResearchGate, letting you access and read them immediately.

AIP | Applied Physics Letters

Trap-assisted large gain in Cu2O/C60 hybrid ultraviolet/visible photodetectors

Lan Liu, Zisheng Su, Qiaoyue Xi, Ge Gao, Wei Yang, Yongxia Zhao, Cunqi Wu, Lidan Wang, and Jingwei Xu

Citation: Applied Physics Letters **108**, 163504 (2016); doi: 10.1063/1.4947581
View online: http://dx.doi.org/10.1063/1.4947581
View Table of Contents: http://scitation.aip.org/content/aip/journal/apl/108/16?ver=pdfcov
Published by the AIP Publishing

Articles you may be interested in

High-performing visible-blind photodetectors based on SnO2/CuO nanoheterojunctions
Appl. Phys. Lett. **107**, 241108 (2015); 10.1063/1.4938129

High-performance ultraviolet detection and visible-blind photodetector based on Cu2O/ZnO nanorods with poly-(N-vinylcarbazole) intermediate layer
Appl. Phys. Lett. **107**, 241113 (2015); 10.1063/1.4938004

Comprehensive studies of response characteristics of organic photodetectors based on rubrene and C60
J. Appl. Phys. **115**, 244506 (2014); 10.1063/1.4885078

Characterization and modeling of a ZnO nanowire ultraviolet photodetector with graphene transparent contact
J. Appl. Phys. **114**, 234505 (2013); 10.1063/1.4854455

Photoconductive gain in solar-blind ultraviolet photodetector based on Mg0.52Zn0.48O thin film
Appl. Phys. Lett. **99**, 242105 (2011); 10.1063/1.3670334

Reuse of AIP Publishing content is subject to the terms at: https://publishing.aip.org/authors/rights-and-permissions. Download to IP: 172.245.157.205 On: Mon, 16 May 2016 09:20:00

Trap-assisted large gain in Cu_2O/C_{60} hybrid ultraviolet/visible photodetectors

Lan Liu,[1,2] Zisheng Su,[3] Qiaoyue Xi,[1,2] Ge Gao,[1,2] Wei Yang,[1] Yongxia Zhao,[1] Cunqi Wu,[1] Lidan Wang,[1,a)] and Jingwei Xu[1,a)]
[1]*The State Key Laboratory of Electroanalytical Chemistry, Changchun Institute of Applied Chemistry, Chinese Academy of Sciences, Changchun 130022, People's Republic of China*
[2]*University of Chinese Academy of Sciences, Beijing 100049, People's Republic of China*
[3]*State Key Laboratory of Luminescence and Applications, Changchun Institute of Optics, Fine Mechanics and Physics, Chinese Academy of Sciences, Changchun 130033, People's Republic of China*

(Received 11 March 2016; accepted 14 April 2016; published online 22 April 2016)

Photomultiplication-type ultraviolet (UV)/visible photodetectors (PDs) are demonstrated in an electrodeposited Cu_2O/C_{60} hybrid structure. These simple organic/inorganic hybrid PDs exhibit external quantum efficiencies (EQEs) of 1.1×10^4% under illumination of 365 nm UV light at −3 V, indicating a large gain of photocurrent for these devices. Such an EQE is one of the highest values among the reported organic/inorganic hybrid PDs at the same voltage. Cu_2O and C_{60} are found to play different roles in realizing the photomultiplication. Copper vacancies are proposed as the defects in the electrodeposited Cu_2O layers, which can trap photogenerated holes. Such trapped holes will trigger the injection of multiple electrons and hence result in the photocurrent gain of the devices while C_{60} primarily acts as a light absorption media to provide free holes. *Published by AIP Publishing.*
[http://dx.doi.org/10.1063/1.4947581]

Photodetectors (PDs) have received much attention due to their wide applications in industrial, military, biological, and environmental applications.[1–3] There are typically two types of PDs, e.g., photodiode- and photomultiplication (PM)-type PDs. For a photodiode-type PD, the external quantum efficiency (EQE) is generally lower than unity due to its limited light absorption efficiency, electron-hole pair (or exciton) dissociation efficiency, and charge-carrier collection efficiency.[4–9] On the other hand, the PM-type PD exhibits an EQE much higher than unity due to the mechanism that one incident photon can trigger more than one hole (or electron) flowing across the PD, indicating a photocurrent gain of this device.[10–12] The active materials of the PM-type PDs can be either inorganic or organic ones. Impact ionization is generally considered as the gain mechanism of inorganic PM-type PDs, and such a mechanism generally requires a high voltage.[13–15] However, impact ionization could not happen in organic materials due to their large binding energy and disordered structure,[16,17] even though large gain has been observed in organic PDs, which is attributed to the trap-assisted incensement of charge carrier injection.[18–20] Due to the thin organic layer used in these devices, the driving voltage was dramatically reduced. Recently, the organic/inorganic hybrid devices have attracted broad interest for PM-type PDs.[21–25] In addition to their similar lower driving voltage as compared with organic counterparts, the energy band structures of these PDs can be easily manipulated by simply revising the molecule structure of the organic materials, providing us unmatchable design flexibility. In these devices, photogenerated electrons are trapped in n-type metal oxides, which reduce hole injection barrier from the cathode and then produce a photocurrent gain. There are rare reports on PM-type PD based on p-type inorganic material/organic hybrid structure. Chen *et al.*[26] have demonstrated a PD with an EQE as high as 8000% at 350 nm and −4.5 V in a p-type CdTe nanoparticles blended polymer-fullerene matrix. However, the driving voltage is desired to be further decreased from the point of view of energy consumption.

Cu_2O is one of the most promising p-type photovoltaic materials owing to its direct bandgap structure, high absorption coefficient, non-toxicity, and cost-efficient production routes.[27–29] The theoretical calculated power conversion efficiency of a Cu_2O solar cell is about 20%.[30] However, the highest efficiency obtained up to now is significantly lower.[30–32] This is attributed to the low quality of the prepared Cu_2O layer that contains a lot of defects (Refs. 33–37) and the short transport length of minority carrier (electrons in Cu_2O).[38,39] However, these defects may act as the traps for photogenerated charge carriers and then manipulate the photoconductivity of the devices, which makes it potentially applicable in PM-type photodetectors. In this work, Cu_2O electrodeposited on ITO substrate is firstly used in PM-type ultraviolet/visible (UV/Vis) PDs. The simple Cu_2O/C_{60} hybrid device shows a high EQE of 1.1×10^4% at 365 nm and a low voltage of −3 V. Such an EQE is one of the highest values among the reported organic/inorganic hybrid PDs at the same wavelength and voltage.[21–26]

Cu_2O layers were synthesized by an electrodeposition method on ITO coated glass substrates with a sheet resistance of 15 Ω/sq in 0.4 M $CuSO_4$ and 3 M lactic acid solution. The PH value of the solution was regulated to 12 by NaOH and the color of the solution turned from light blue into dark blue. The deposition was carried out in a configured glass cell at 60 °C, in which the ITO substrate, a platinum plate, and an Ag/AgCl electrode in a saturated KCl solution served as the working electrode, the counter electrode, and the reference electrode, respectively. During the electrodeposition, the potential was set to be of −0.3 V vs the reference electrode and the duration of the depositions was varied from 60 to 150 s. Devices were fabricated by thermal evaporating

a)Authors to whom correspondence should be addressed. Electronic addresses: wangld@ciac.ac.cn and jwxu@ciac.ac.cn

Reuse of AIP Publishing content is subject to the terms at: https://publishing.aip.org/authors/rights-and-permissions. Download to IP: 172.245.157.205 On: Mon, 16 May 2016 09:20:00

60 nm C_{60}, 10 nm 4,7-diphenyl-1,10-phenanthroline (Bphen), and 100 nm Al in sequence onto the Cu_2O layers in a vacuum chamber at a pressure of 5×10^{-4} Pa without breaking vacuum, and substrates were held at room temperature during this process. Deposition rate and layer thickness were monitored *in situ* using oscillating quartz monitors. Evaporation rates were kept at 1 Å/s for C_{60} and Bphen and 10 Å/s for Al cathode. X-ray diffraction (XRD) patterns were measured with a Rigaku D/Max-2500 diffractometer using Cu Kα radiation ($\lambda = 1.54$ Å). Absorption spectra were recorded on a Shimadzu UV-3101 spectrophotometer in a transmittance arrangement with a bare ITO glass as the reference. Scanning electron microscopy (SEM) images were measured by a Philips-FEI XL30-SFEG scanning electron microscopy. X-ray photoelectron spectroscopy (XPS) measurements were taken on an ESCALAB-MKII 250 photoelectron spectrometer (VG Co.) with Al Kα X-ray radiation as the source for excitation. Current-voltage (*J-V*) characteristics of the devices were measured with a Keithley 2400 source meter. The EQE spectra were performed with a Stanford SR803 lock-in amplifier under monochromatic illumination.

Figures 1(a)–1(d) show the SEM images of Cu_2O layers on ITO substrates with deposition times of 60, 90, 120, and 150 s and their corresponding cross-sectional ones in (Figs. 1(e)–1(h)), respectively. No complete Cu_2O film but Cu_2O particles are formed within the deposition time of 150 s. SEM images of these Cu_2O particles with a large magnified scale are displayed in Fig. S1 (in Ref. 40). The Cu_2O particles deposited for 60 s are uniform and semisphere with an average diameter of about 2 μm. When the deposition time increases to 90 s, both the morphology and density of Cu_2O particles are almost unchanged, but the diameter increases to about 3 μm. Further increase in the deposition time results in an increase of the particle density with the same diameter but a gradual change of the morphology from semisphere to truncated octahedra. During this deposition period, the height of the particles always keeps at about 1 μm, indicating that the growth of Cu_2O particle is primary in the landscape orientation.

XRD patterns of the Cu_2O layers with different deposition times are plotted in Fig. S2 (in Ref. 40). Three peaks at 2θ of ca. 29.78°, 36.81°, and 42.89° are observed, which can be assigned to the (110), (111), and (200) planes of Cu_2O crystal, respectively, indicating that the Cu_2O has the pure cuprous structure (JCPDF No. 05-0667). No other phase, such as CuO, is detected.

Cu_2O/C_{60} hybrid devices were fabricated based on these different Cu_2O layers. Figure S3 (in Ref. 40) shows the cross-sectional SEM images of the entire device. It can be found that the Cu_2O particles are fully covered by the upper organic and Al layers. Figure 2 depicts the EQE spectra of the Cu_2O/C_{60} hybrid devices with different Cu_2O layers at zero bias. The EQE spectra have the same sharp with a response peak at about 360 nm and a shoulder at about 450 nm, suggesting that these devices can be applied as UV/Vis PDs. Among these PDs, the device with 90 s Cu_2O exhibits the highest EQE of about 28%, corresponding to a response of 82 mA/W at 360 nm.

Figure 3 illuminates the absorption spectra of 90 s Cu_2O, 60 nm C_{60}, and their hybrid films. Although both Cu_2O and C_{60} absorb at the UV/Vis region, the absorption intensity of Cu_2O is significantly lower than that of C_{60} due to its low coverage, as shown in Fig. 1. The absorption of the Cu_2O/C_{60} hybrid film is almost the sum of the two individuals, and the abnormal spectra near 300 nm should be attributed to the experiment error due to the high absorption of ITO in this region and the difference between ITO substrates. Due to the lower absorption of Cu_2O, the response of the Cu_2O/C_{60} hybrid devices may primarily come from C_{60}. To validate this hypothesis, a reference device with the structure of ITO/MoO_3 (2 nm)/C_{60} (60 nm)/Bphen (10 nm)/Al is fabricated. In this device, MoO_3 forms a Schottky contact with C_{60} and the photocurrent is only contributed from the absorption of C_{60}.[41] Interestingly, the shape of EQE spectrum of this device is the same to those of the Cu_2O/C_{60} hybrid devices, as shown in Fig. S4 (in Ref. 40). This indicates that the response of the hybrid devices primarily results from the absorption of C_{60}.

Figure S5 (in Ref. 40) draws the dark current of the Cu_2O/C_{60} hybrid devices with different Cu_2O layers. It can be found that all the devices have a similar dark current curve with a typical diode character. The rectification ratio of these devices reaches to the order of 10^3 at ±3 V. It should be noted that the dark current is higher than other

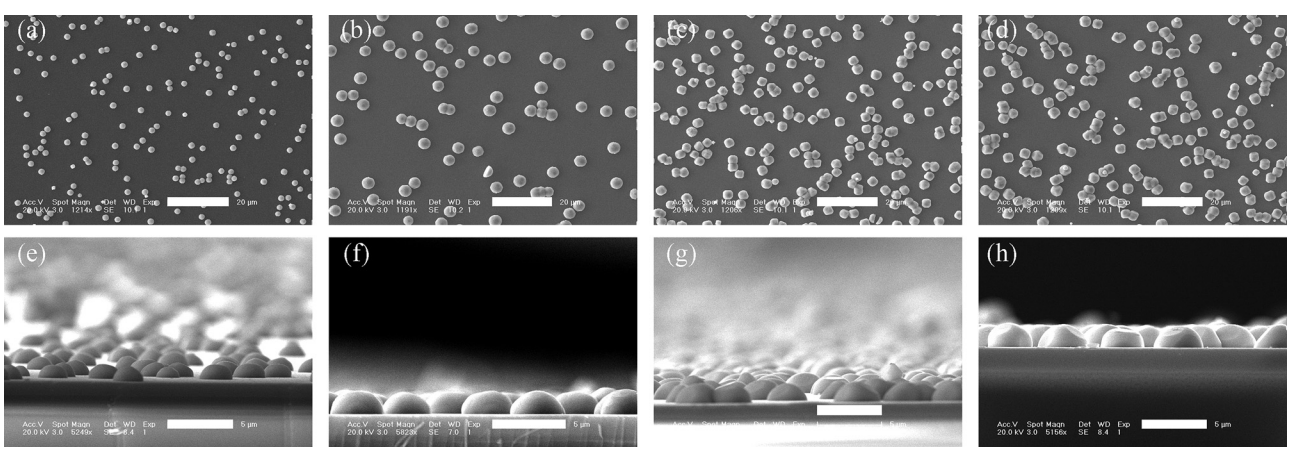

FIG. 1. SEM images of Cu_2O layer on ITO substrates with deposition times of (a) 60, (b) 90, (c) 120, and (d) 150 s and their corresponding cross-sectional SEM images (e)–(h), respectively. The scale bars in the upper and lower images indicate a length of 20 and 5 μm, respectively.

Reuse of AIP Publishing content is subject to the terms at: https://publishing.aip.org/authors/rights-and-permissions. Download to IP: 172.245.157.205 On: Mon, 16 May 2016 09:20:00

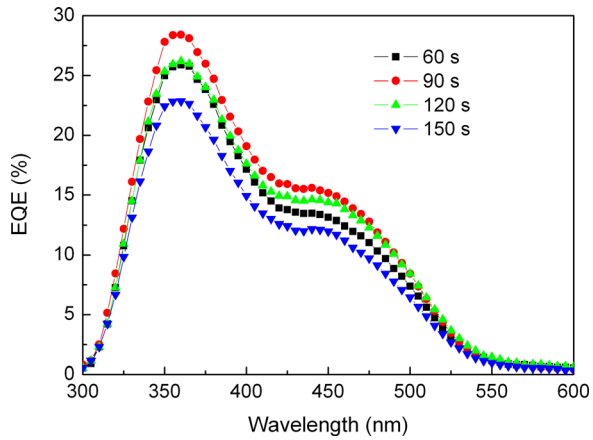

FIG. 2. EQE spectra of the ITO/Cu_2O/C_{60}/Bphen/Al hybrid devices with different Cu_2O layers at zero bias.

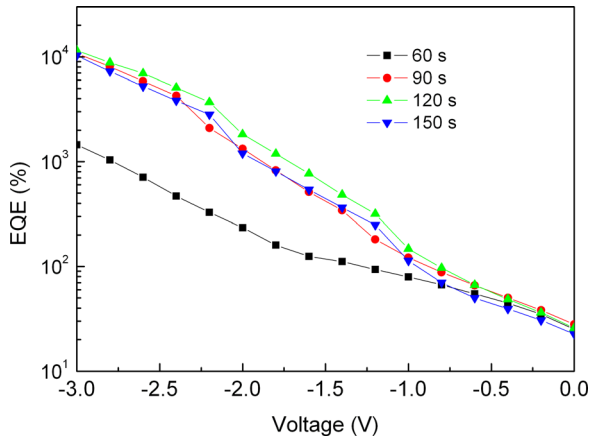

FIG. 4. EQE as a function of voltage of the ITO/Cu_2O/C_{60}/Bphen/Al hybrid devices with different Cu_2O layers.

reported organic/inorganic hybrid PDs,[21–26] which is attributed to the direct contact between ITO and C_{60}.

The photocurrent of a PD can increase with the applied reverse voltage, and the difference between the photodiode- and PM-type PDs is that the photocurrent tends to saturate at a low voltage with an EQE less than unity for the former while it can increase continuously with the voltage to an EQE dramatically higher than unity for the latter. The photocurrent of the Cu_2O/C_{60} hybrid devices is measured under illumination of a 365 nm UV light with an intensity of 1.2 mW/cm^2. The calculated EQEs as a function of voltage are plotted in Fig. 4. The EQEs at zero bias are in the range of 22%–28%, which are coinciding with the ones measured from their EQE spectra. The EQEs increase rapidly with the voltage and excess 100% at a low voltage of only −1 V. All the devices achieve a maximum EQE of about 1.1×10^4% at −3 V, corresponding to a photocurrent gain of 110, except the device with a 20 s Cu_2O. This finding indicates that these hybrid devices can be used as high efficient PM-type PDs, and this EQE is one of the highest values among the reported organic/inorganic hybrid PDs at the same wavelength and voltage.[21–26]

The response speed is another merit-of-figure for a PD. Figure S6 (in Ref. 40) shows the photocurrent transient measurement by periodically switching on and off the 365 nm UV light with an intensity of 1.2 mW/cm^2 at zero bias. The rising and decaying rates of the photocurrent are pretty rapid and faster than the limit of our measurement setup of 50 ms. Besides, we have found that the photocurrent of the Cu_2O/C_{60} hybrid UV/Vis PDs can increase linearly with the intensity of the UV light in the range from 0.038 to 1.2 mW/cm^2, as shown in Fig. S7 (in Ref. 40). Such a character is important for the application of PDs.

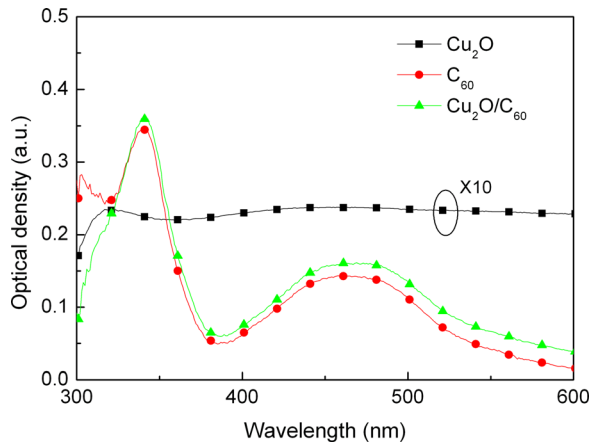

FIG. 3. Absorption spectra of 90 s Cu_2O, 60 nm C_{60}, and their hybrid films.

To clarify the role of Cu_2O and C_{60} in the PDs, the photoresponse of the ITO/MoO_3/C_{60}/Bphen/Al reference device at different voltages is investigated. Figure S8 (in Ref. 40) shows the EQE as a function of voltage under the illumination of the 365 nm UV light with an intensity of 1.2 mW/cm^2. The EQE increases from 59% at zero bias to 173% at −3 V, indicating a gain of photocurrent for this device. Similar photocurrent gain has been found in ITO/poly(3,4-ethylenedioxythiophene): poly(styrenesulfonate) (PEDOT:PSS)/C_{60}/bathocuproine/Al device by Huang and Yang, which is attributed to the disordered structure of C_{60} and the charge trapping at the PEDOT:PSS/C_{60} interface.[42] However, we can also find that the gain of the reference device is significantly lower than that of Cu_2O/C_{60} hybrid devices which exhibit EQEs as high as 1.1×10^4%, as shown in Fig. 4. This suggests that Cu_2O may play a more important role in determining the gain of the hybrid devices.

Various types of copper vacancy, such as simple and split copper vacancies, have been proposed to exist in Cu_2O.[33–37] Although the primary type of vacancy is still under debate, all these vacancies can act as hole traps because they introduce defect levels above the valence-band maximum of Cu_2O. One of the ways to form the copper vacancies is the outward migration of copper atoms toward the surface and finally oxidized to CuO.[43] Figure 5 shows the XPS spectrum of Cu_2O layer with the deposition time of 90 s. It can be found that the binding energies of the Cu $2p_{1/2}$ and Cu $2p_{3/2}$ are 953 and 933 eV, respectively, which are the characteristics of Cu^+.[44] Meanwhile, weak satellite peaks of Cu 2p at 960 and 943 eV are observed, which are evident and diagnostic of an open $3d^9$ shell of Cu^{2+}.[44] These findings indicate that the surface of Cu_2O particles is partially oxidized to CuO, which suggests that there may be a high density of copper vacancy in the Cu_2O particles. The fact that the XRD does not show evidence of CuO phase indicates that CuO is present only on the surface of Cu_2O particles. Thus the photocurrent gain of the Cu_2O/C_{60} hybrid PDs can be understood, as shown in the

Reuse of AIP Publishing content is subject to the terms at: https://publishing.aip.org/authors/rights-and-permissions. Download to IP: 172.245.157.205 On: Mon, 16 May 2016 09:20:00

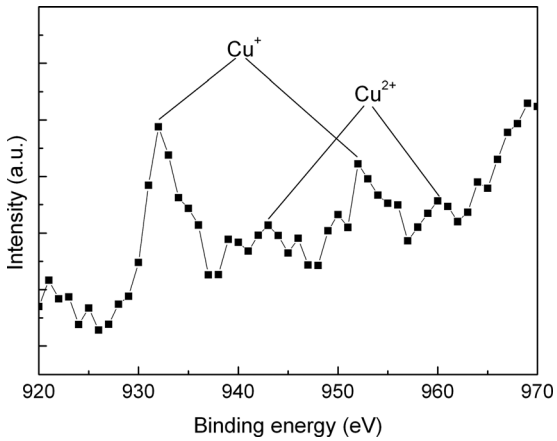

FIG. 5. XPS spectrum of 90 s Cu_2O deposited on an ITO substrate.

schematic energy band diagrams in Fig. S9 (in Ref. 40). Under dark, electron injection from ITO is blocked by Cu_2O while hole injection from Al is blocked by Bphen due to their high injection barriers. Under illumination and reverse bias, excitons form in C_{60} molecules and then dissociate to free holes and electrons at the Cu_2O/C_{60} interface. The photogenerated holes are trapped by the copper vacancies in Cu_2O during their transport to ITO electrode. The trapped holes cause a large band bending, which dramatically reduces electron injection barrier from ITO and they can be tunneling injected. Since one trapped hole can trigger more than one electron injected from ITO anode, an apparent photocurrent gain is found in the Cu_2O/C_{60} hybrid PDs. In view of this, we can conclude that the role of Cu_2O in these PDs is primarily to provide hole traps while C_{60} to absorb the incident photons and generate free charge carriers.

In summary, large Cu_2O particles are prepared on ITO substrate by an electrodeposition method and applied to fabricate organic/inorganic hybrid UV/Vis PDs. The simple Cu_2O/C_{60} PDs present a high EQE of 1.1×10^4% under illumination of 365 nm UV light at −3 V, which is one of the highest values among the reported organic/inorganic hybrid UVPDs at the same wavelength and voltage. Copper vacancies are proposed as the defects in the electrodeposited Cu_2O layers. Such defects can trap photogenerated holes, which result in a decrease of electron injection barrier from ITO anode and hence the photocurrent gain of the PDs, while C_{60} only acts as a light absorption media. This provides us a design flexibility to construct Vis, near-infrared, or even panchromatic PM-type PDs by simply changing the light absorption materials. The reported high performance PDs may have the great potential to apply in a wide range of field, and this work provides a simple and low cost method to fabricate high performance PM-type PDs.

This work was supported by the National Natural Science Foundation of China (61504145 and 61575192).

[1]M. Razeghi and A. Rogalski, J. Appl. Phys. **79**, 7433 (1996).
[2]H. Dong, H. Zhu, Q. Meng, X. Gong, and W. Hu, Chem. Soc. Rev. **41**, 1754 (2012).
[3]K. J. Baeg, M. Binda, D. Natali, M. Caironi, and Y. Y. Noh, Adv. Mater. **25**, 4267 (2013).
[4]X. Gong, M. Tong, Y. Xia, W. Cai, J. S. Moon, Y. Cao, G. Yu, C.-L. Shieh, B. Nilsson, and A. J. Heeger, Science **325**, 1665 (2009).
[5]Z. Su, W. Li, B. Chu, T. Li, J. Zhu, G. Zhang, F. Yan, X. Li, Y. Chen, and C. S. Lee, Appl. Phys. Lett. **93**, 103309 (2008).
[6]Y. Y. Lin, C. W. Chen, W. C. Yen, W. F. Su, C. H. Ku, and J. J. Wu, Appl. Phys. Lett. **92**, 233301 (2008).
[7]H. G. Li, G. Wu, M. M. Shi, L. G. Yang, H. Z. Chen, and M. Wang, Appl. Phys. Lett. **93**, 153309 (2008).
[8]L. Wang, D. Zhao, Z. Su, F. Fang, B. Li, Z. Zhang, D. Shen, and X. Wang, Org. Electron. **11**, 1318 (2010).
[9]Y. Kim, S. J. Kim, S. P. Cho, B. H. Hong, and D. J. Jang, Sci. Rep. **5**, 12345 (2015).
[10]Y. Jin, J. Wang, B. Sun, J. C. Blakesley, and N. C. Greenham, Nano Lett. **8**, 1649 (2008).
[11]V. Q. Dang, T. Q. Trung, D. I. Kim, L. T. Duy, B. U. Hwang, D. W. Lee, B. Y. Kim, L. D. Toan, and N. E. Lee, Small **11**, 3054 (2015).
[12]Z. Jin, L. Gao, Q. Zhou, and J. Wang, Sci. Rep. **4**, 4268 (2014).
[13]A. Nevet, A. Hayat, and M. Orenstein, Opt. Lett. **36**, 725 (2011).
[14]O. Hayden, R. Agarwal, and C. M. Lieber, Nat. Mater. **5**, 352 (2006).
[15]D. Y. Kim, J. Ryu, J. Manders, J. Lee, and F. So, ACS Appl. Mater. Interfaces **6**, 1370 (2014).
[16]J. Reynaert, V. I. Arkhipov, P. Heremans, and J. Poortmans, Adv. Funct. Mater. **16**, 784 (2006).
[17]L. A. A. Pettersson, L. S. Roman, and O. Inganäs, J. Appl. Phys. **89**, 5564 (2001).
[18]M. Hiramoto, T. Imahigashi, and M. Yokoyama, Appl. Phys. Lett. **64**, 187 (1994).
[19]L. Li, F. Zhang, J. Wang, Q. An, Q. Sun, W. Wang, J. Zhang, and F. Teng, Sci. Rep. **5**, 9181 (2015).
[20]W. Wang, F. Zhang, L. Li, M. Gao, and B. Hu, ACS Appl. Mater. Interfaces **7**, 22660 (2015).
[21]F. Guo, B. Yang, Y. Yuan, Z. Xiao, Q. Dong, Y. Bi, and J. Huang, Nat. Nanotechnol. **7**, 798 (2012).
[22]D. Shao, M. Yu, H. Sun, G. Xin, J. Lian, and S. Sawyer, ACS Appl. Mater. Interfaces **6**, 14690 (2014).
[23]Y. Fang, F. Guo, Z. Xiao, and J. Huang, Adv. Opt. Mater. **2**, 348 (2014).
[24]R. Dong, C. Bi, Q. Dong, F. Guo, Y. Yuan, Y. Fang, Z. Xiao, and J. Huang, Adv. Opt. Mater. **2**, 549 (2014).
[25]A. A. Hussain, A. R. Pal, and D. S. Patil, Appl. Phys. Lett. **104**, 193301 (2014).
[26]H.-Y. Chen, M. K. F. Lo, G. Yang, H. G. Monbouqwette, and Y. Yang, Nat. Nanotechnol. **3**, 543 (2008).
[27]C. Malerba, F. Biccari, C. L. A. Ricardo, M. D'Incau, P. Scardi, and A. Mittiga, Sol. Energy Mater. Sol. Cells **95**, 2848 (2011).
[28]X. Liu, H. Du, P. Wang, T. T. Lim, and X. W. Sun, J. Mater. Chem. C **2**, 9536 (2014).
[29]F. A. Akgul, G. Akgul, N. Yildirim, H. E. Unalan, and R. Turan, Mater. Chem. Phys. **147**, 987 (2014).
[30]A. Mittiga, E. Salza, F. Sarto, M. Tucci, and R. Vasanthi, Appl. Phys. Lett. **88**, 163502 (2006).
[31]M. Izaki, T. Saito, T. Ohata, K. Murata, B. M. Fariza, J. Sasano, T. Shinagawa, and S. Watase, ACS Appl. Mater. Interfaces **4**, 3558 (2012).
[32]T. Minami, Y. Nishi, and T. Miyata, Appl. Phys. Express **8**, 022301 (2015).
[33]O. Porat and I. Riess, Solid State Ionics **81**, 29 (1995).
[34]D. O. Scanlon, B. J. Morgan, and G. W. Watson, Phys. Rev. Lett. **103**, 096405 (2009).
[35]G. K. Paul, Y. Nawa, H. Sato, T. Sakurai, and K. Akimoto, Appl. Phys. Lett. **88**, 141901 (2006).
[36]L. Y. Isseroff and E. A. Carter, Chem. Mater. **25**, 253 (2013).
[37]Y. Yang, J. Han, X. Ning, W. Cao, W. Xu, and L. Guo, ACS Appl. Mater. Interfaces **6**, 22534 (2014).
[38]K. P. Musselman, A. Wisnet, D. C. Iza, H. C. Hesse, C. Scheu, J. L. MacManus-Driscoll, and L. Schmidt-Mende, Adv. Mater. **22**, E254 (2010).
[39]Y. Liu, H. K. Turley, J. R. Tumbleston, E. T. Samulski, and R. Lopez, Appl. Phys. Lett. **98**, 162105 (2011).
[40]See supplementary material at http://dx.doi.org/10.1063/1.4947581 for details about SEM, XRD, EQE, dark current, photoresponse, and schematic energy band diagrams of the devices (Figures S1–S9).
[41]M. Zhang, Irfan, H. Ding, Y. Gao, and C. W. Tang, Appl. Phys. Lett. **96**, 183301 (2010).
[42]J. Huang and Y. Yang, Appl. Phys. Lett. **91**, 203505 (2007).
[43]Z. Grzesik and M. Migdalska, High Temp. Mater. Processes **30**, 277 (2011).
[44]M. Yin, C. K. Wu, Y. Lou, C. Burda, J. T. Koberstein, Y. Zhu, and S. O'Brien, J. Am. Chem. Soc. **127**, 9506 (2005).

Reuse of AIP Publishing content is subject to the terms at: https://publishing.aip.org/authors/rights-and-permissions. Download to IP: 172.245.157.205 On: Mon, 16 May 2016 09:20:00

View publication stats